Comput Geosci (2012) 16:677–690
DOI 10.1007/s10596-012-9277-3

ORIGINAL PAPER

Discontinuous Galerkin method for two-component liquid–gas porous media flows

Alexandre Ern · Igor Mozolevski

Received: 21 September 2011 / Accepted: 17 January 2012 / Published online: 2 March 2012

Abstract We consider two-component (typically, water and hydrogen) compressible liquid–gas porous media flows including mass exchange between phases possibly leading to gas-phase (dis)appearance, as motivated by hydrogen production in underground repositories of radioactive waste. Following recent work by Bourgeat, Jurak, and Smaï, we formulate the governing equations in terms of liquid pressure and dissolved hydrogen density as main unknowns, leading mathematically to a nonlinear elliptic–parabolic system of partial differential equations, in which the equations degenerate when the gas phase disappears. We develop a discontinuous Galerkin method for space discretization, combined with a backward Euler scheme for time discretization and an incomplete Newton method for linearization. Numerical examples deal with gas-phase (dis)appearance, ill-prepared initial conditions, and heterogeneous problem with different rock types.

Keywords Two-phase two-component flows · Porous media · Elliptic–parabolic system · Discontinuous Galerkin methods

A. Ern (✉)
Université Paris-Est, CERMICS, Ecole des Ponts ParisTech,
6 & 8 Av. B. Pascal, 77455 Marne-la-Vallée cedex 2, France
e-mail: ern@cermics.enpc.fr

I. Mozolevski
Departamento de Matemática, Universidade Federal
de Santa Catarina, 88040900 Florianópolis,
Santa Catarina, Brazil
e-mail: Igor.Mozolevski@mtm.ufsc.br

Mathematics Subject Classifications (2010) MSC
76S05 · 76T99 · 65M60 · 65N30

1 Introduction

Multicomponent multiphase porous media flows are encountered in several applications including petroleum engineering and various hydrology models related, e.g., to agricultural engineering and groundwater remediation. Such flows have received an enhanced attention recently in connection with gas sequestration and the disposal of radioactive waste in underground repositories. This last application actually constitutes the main motivation for the present work. In such repositories, the corrosion of metallic components, and also marginally the radiolysis of water, leads to hydrogen production. An important issue in the design and safety analysis of the underground repository is then to understand and predict the migration of hydrogen through the host rock. A typical model to describe this situation is to consider a two-phase (liquid and gas), two-component (water and hydrogen) flow. During the simulation, the gas phase is generally not present in the whole domain, as hydrogen gradually penetrates into the host rock which is initially saturated. When both phases are present, the hydrogen component is assumed to be in thermodynamic equilibrium between both phases, and in the context of moderate hydrogen concentrations, this equilibrium is described by the linear Henry law for hydrogen dissolution. For simplicity, we assume herein that water does not vaporize, which is a reasonable assumption in the present context. Additionally, the compressibility of the gas phase must be accounted for.

Multicomponent multiphase porous media flows are described by well-established models covered in several monographs, see, e.g., Bear [6], Chavent and Jaffré [10], Helmig [20], Marle [26], and Peaceman [30]. There is a satisfactory mathematical theory for incompressible two-phase flows hinging on the theory of elliptic–parabolic partial differential equations (PDEs), see, e.g., [2, 7, 23, 24, 28]. Recent mathematical results in the compressible case can be found in [3, 25] without mass exchange between phases and in [27, 33, 34] with mass exchange.

The possibility of gas-phase disappearance rises the issue of selecting the main unknowns in the governing equations since, typically, the phase saturations are not appropriate for that purpose. Following [8, 32], we select here the liquid pressure together with the dissolved hydrogen density. This choice is motivated by the fact that the liquid phase is always present in the whole domain, while the dissolved hydrogen density is always well-defined, regardless of the presence of a gas phase. As observed in [22], Henry's law can be used within a formulation with complementary constraints to determine the presence of the gas phase. Here, as in [8, 32], we adopt the simpler approach where the gas-phase saturation is recovered from the main unknowns using the reciprocal function of the capillary pressure extended by zero. An alternative approach to phase disappearance (where both phases can disappear in different parts of the domain) is discussed in [1, 29].

The goal of the present work is to design and evaluate numerically a discontinuous Galerkin (dG) method for two-component compressible liquid–gas porous media flows including mass exchange between phases. The dG method is used for space discretization, in conjunction with a backward Euler scheme for time discretization and an inexact Newton solver for linearization. Of special interest in the numerical evaluation of the dG method are test cases featuring gas-phase (dis)appearance, ill-prepared initial conditions, and heterogeneous problems with different rock types. Introduced 40 years ago, dG methods have experienced a vigorous development over the last decade in many fields of engineering. Attractive features offered by dG methods include the possibility of enforcing locally basic conservation principles, the flexibility in designing the mesh and local degrees of freedom, and the ability to enforce interface conditions in the context of multi-domain problems. We refer to [4, 14] for a unified analysis of dG methods and to recent monographs on the subject [12, 21, 31]. DG methods for incompressible two-phase porous media flows without inter-phase mass exchange have been developed, e.g., in [5, 13, 15, 16, 18], but, to our knowledge, this is the first time where compressible flows with inter-phase mass exchange are covered.

This paper is organized as follows: In Section 2, we present the governing equations and formulate the mathematical model. In Section 3, we describe the numerical method and, in particular, design the dG method for space discretization. Finally, in Section 4, we present the numerical results and we draw some conclusions in Section 5.

2 Problem setting

In this section, we first present the governing equations in their basic form. Then, we specify the choice of main unknowns and derive the mathematical model.

2.1 Governing equations

We assume that the porous medium is isothermal and undeformable. We adopt the terminology of our targeted application related to hydrogen production within geological repositories of radioactive waste. The two phases are indicated by a subscript $\alpha \in \{\mathrm{l}, \mathrm{g}\}$ referring to liquid and gas, respectively. We consider two components, indicated by a superscript $\beta \in \{w, h\}$ referring to water and hydrogen, respectively.

The mass conservation equation for each component $\beta \in \{w, h\}$ can be written as

$$\Phi \sum_{\alpha\in\{\mathrm{l},\mathrm{g}\}} \partial_t \left(s_\alpha \varrho_\alpha^\beta\right) + \sum_{\alpha\in\{\mathrm{l},\mathrm{g}\}} \nabla\cdot\left(\varrho_\alpha^\beta \mathbf{q}_\alpha + \mathbf{j}_\alpha^\beta\right) = F^\beta, \tag{1}$$

where Φ denotes the porosity, s_α the saturation of phase α, ϱ_α^β the density of component β in phase α, $\mathbf{q}_\alpha$ the volumetric flow rate for phase α, $\mathbf{j}_\alpha^\beta$ the mass diffusion flux of component β in phase α, and F^β the source term of component β. The volumetric flow rate of each phase is obtained from the Darcy–Muskat law in the form

$$\mathbf{q}_\alpha = -K\lambda_\alpha(s_\alpha)\nabla p_\alpha, \qquad \alpha \in \{\mathrm{l}, \mathrm{g}\}, \tag{2}$$

where K denotes the absolute permeability of the medium (taken to be scalar-valued for simplicity), λ_α the mobility of phase α (assumed to be a given function of the saturation s_α such that λ_α vanishes if the phase α is absent), and p_α the pressure of phase α. For simplicity, gravity forces are neglected in Eq. 2. The phase saturations take values in [0, 1] (in hydrogeology models, they often take values in a subinterval of [0, 1] depending on residual saturations of both phases, cf. Section 4) and are such that

$$s_\mathrm{l} + s_\mathrm{g} = 1. \tag{3}$$

Furthermore, assuming that the gas phase is the non-wetting phase, the phase pressures are such that

$$p_{\mathrm{g}} = p_{\mathrm{l}} + \pi(s_{\mathrm{g}}), \tag{4}$$

where $\pi : [0, 1) \to [\pi(0), +\infty)$ denotes the capillary pressure (assumed to be a given function of the gas saturation). The quantity $\pi(0)$ denotes the possibly nonzero entry pressure.

Concerning the water component, we assume incompressibility in the liquid phase, and we neglect water vaporization. As a result,

$$\varrho_{\mathrm{l}}^{w} = \varrho_{\mathrm{l}}^{\mathrm{std}}, \qquad \varrho_{\mathrm{g}}^{w} = 0, \tag{5}$$

where $\rho_{\mathrm{l}}^{\mathrm{std}}$ denotes the standard water density at the given temperature of the medium. Concerning the hydrogen component, we assume the ideal gas law in the gas phase and that hydrogen-phase changes are in thermodynamic equilibrium as governed by Henry's law. This leads to

$$\varrho_{\mathrm{g}}^{h} = C_{\mathrm{g}} p_{\mathrm{g}}, \qquad C_{\mathrm{g}} = \frac{M^h}{RT}, \tag{6}$$

and

$$\varrho_{\mathrm{l}}^{h} = C_h p_{\mathrm{g}}, \qquad C_h = H M^h, \tag{7}$$

where M^h denotes the hydrogen molar mass, R the universal gas constant, T the (absolute) temperature, and H the (temperature-dependent) constant in Henry's law. Furthermore, the hydrogen diffusion flux in the liquid phase, $\mathbf{j}_{\mathrm{l}}^{h}$, is evaluated using a Fick-type law in the form

$$\mathbf{j}_{\mathrm{l}}^{h} = -\Phi s_{\mathrm{l}} D_{\mathrm{l}}^{h} \nabla \varrho_{\mathrm{l}}^{h}, \tag{8}$$

where D_{l}^{h} denotes the (temperature-dependent) molecular diffusion coefficient of hydrogen in the liquid phase. Since for a two-component system, the diffusion fluxes in the liquid phase satisfy $\sum_{\beta\in\{w,h\}} \mathbf{j}_{\mathrm{l}}^{\beta} = 0$, we infer $\mathbf{j}_{\mathrm{l}}^{w} = -\mathbf{j}_{\mathrm{l}}^{h}$. The use of the Fick-type law (Eq. 8) using density, and not concentration, gradients and neglecting cross-diffusion effects is reasonable as long as the hydrogen component is diluted in the liquid phase.

To sum up, the above simplifying assumptions allow us to recast the mass conservation equations (1) for both components as

$$\Phi \varrho_{\mathrm{l}}^{\mathrm{std}} \partial_t s_{\mathrm{l}} + \nabla \cdot \left(\varrho_{\mathrm{l}}^{\mathrm{std}} \mathbf{q}_{\mathrm{l}} - \mathbf{j}_{\mathrm{l}}^{h} \right) = F^{w}, \tag{9a}$$

$$\Phi \partial_t \left(\varrho_{\mathrm{l}}^{h} s_{\mathrm{l}} + C_{\mathrm{g}} p_{\mathrm{g}} s_{\mathrm{g}} \right) + \nabla \cdot \left(\varrho_{\mathrm{l}}^{h} \mathbf{q}_{\mathrm{l}} + C_{\mathrm{g}} p_{\mathrm{g}} \mathbf{q}_{\mathrm{g}} + \mathbf{j}_{\mathrm{l}}^{h} \right) = F^{h}. \tag{9b}$$

2.2 Mathematical model

Owing to the possible disappearance of the gas phase in some parts of the computational domain that are a priori unknown, it is not appropriate to select any of the saturations or the gas pressure as one of the main unknowns of the mathematical model. Indeed, the saturations vanish identically, or are identically equal to one, in those regions where only the liquid phase is present, while the gas pressure is not even defined in those regions. Following the recent ideas of Smaï [32] (see also Bourgeat, Jurak, and Smaï [8] for a slightly different choice), we select as main unknowns of the mathematical model the liquid pressure p_{l} (since the liquid phase is always present throughout the domain) and the dissolved hydrogen density ϱ_{l}^{h}. In what follows, we set

$$y = (y_1, y_2), \qquad y_1 := p_{\mathrm{l}}, \qquad y_2 := \varrho_{\mathrm{l}}^{h}. \tag{10}$$

The mass conservation equations (9) can then be recast into the form

$$\partial_t b_1(y) - \nabla \cdot (A_{11}(y) \nabla y_1 + A_{12}(y) \nabla y_2) = F_1, \tag{11a}$$

$$\partial_t b_2(y) - \nabla \cdot (A_{21}(y) \nabla y_1 + A_{22}(y) \nabla y_2) = F_2, \tag{11b}$$

or, in more compact form, for all $i \in \{1, 2\}$,

$$\partial_t b_i(y) - \sum_{j\in\{1,2\}} \nabla \cdot (A_{ij}(y) \nabla y_j) = F_i, \tag{12}$$

with source terms $F_1 := F^{w}$, $F_2 := F^{h}$, and

$$b_1(y) = -\Phi \varrho_{\mathrm{l}}^{\mathrm{std}} s_{\mathrm{g}}(y), \tag{13a}$$

$$b_2(y) = \Phi a(s_{\mathrm{g}}(y)) y_2, \tag{13b}$$

$$A_{11}(y) = \varrho_{\mathrm{l}}^{\mathrm{std}} K \lambda_{\mathrm{l}}(1 - s_{\mathrm{g}}(y)), \tag{13c}$$

$$A_{12}(y) = -\Phi(1 - s_{\mathrm{g}}(y)) D_{\mathrm{l}}^{h}, \tag{13d}$$

$$A_{21}(y) = y_2 K \lambda_{\mathrm{l}}(1 - s_{\mathrm{g}}(y)), \tag{13e}$$

$$A_{22}(y) = y_2 K \lambda_{\mathrm{g}}(s_{\mathrm{g}}(y)) \omega C_h^{-1} + \Phi(1 - s_{\mathrm{g}}(y)) D_{\mathrm{l}}^{h}, \tag{13f}$$

where $\omega = \frac{C_{\mathrm{g}}}{C_h}$ and $a(s) = 1 + (\omega - 1)s$. Finally, the gas saturation is recovered from

$$s_{\mathrm{g}}(y) = \pi^{-1}\left(\frac{y_2}{C_h} - y_1 \right), \tag{14}$$

where $\pi^{-1} : \mathbb{R} \to [0, 1)$ denotes the extension by zero to $\mathbb{R}$ of the inverse function of the capillary pressure π, cf Fig. 1. We observe that s_{g} is a continuous function

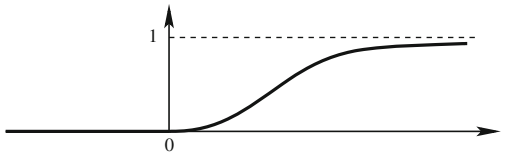

Fig. 1 Function $\pi^{-1}:\mathbb{R}\to[0,1)$ used to recover the gas saturation

of y; this function is actually differentiable if the van Genuchten model is considered for the capillary pressure, as is often the case in hydrogeology and is actually the case in our numerical experiments presented in Section 4 below. If the Brooks–Corey model is used instead, the function π^{-1} is not differentiable at the entry pressure $\pi(0)$, and a semi-smooth version of the linearization procedure described in Section 3.1 needs to be considered.

The governing equations (12), supplemented with Eqs. 13 and 14, are posed in the computational domain Ω which we assume to be a bounded, open, polyhedral domain in $\mathbb{R}^d$, $d\geq 1$, with boundary denoted by $\partial\Omega$ and outward unit normal by $\mathbf{n}$. Dirichlet and Neumann boundary conditions are enforced at the boundary. Given a partition of $\partial\Omega$ into $\partial\Omega_{\mathrm{D}}\cup\partial\Omega_{\mathrm{N}}$, we enforce on $\partial\Omega_{\mathrm{D}}$ the value $y=y_{\mathrm{D}}$, and on $\partial\Omega_{\mathrm{N}}$, we enforce $\mathbf{n}\cdot\boldsymbol{\sigma}_i(y)=\sigma_i$ for all $i\in\{1,2\}$, where the total fluxes $\boldsymbol{\sigma}_i$ are defined as

$$\boldsymbol{\sigma}_i(y)=-(A_{i1}(y)\nabla y_1+A_{i2}(y)\nabla y_2). \tag{15}$$

It is possible to consider a setting where the partition into Dirichlet and Neumann boundaries depends on the component $i\in\{1,2\}$, but this generality is not needed for the test cases envisaged herein. Finally, initial conditions are imposed on y in the form $y(x,0)=y_0$ for all $x\in\Omega$.

Equation 11a is a parabolic equation in y_1 (since the liquid phase is always present) that degenerates into an elliptic equation if the gas phase disappears. Equation 11b is a parabolic equation in y_2 that degenerates into an elliptic equation if there is no dissolved hydrogen. Therefore, Eq. 11a is loosely termed the "pressure equation" and Eq. 11b the "hydrogen equation." To examine the coupled system, we write it in nondimensional form. Let $y_1=p_0\overline{y}_1$ and $y_2=C_hp_0\overline{y}_2$, where p_0 denotes a reference pressure. Dividing Eq. 11a by $\varrho_{\mathrm{l}}^{\mathrm{std}}$ and Eq. 11b by C_hp_0 yields

$$\partial_t\overline{b}_1(\overline{y})-\nabla\cdot\left(\overline{A}_{11}(\overline{y})\nabla\overline{y}_1+\overline{A}_{12}(y)\nabla\overline{y}_2\right)=\overline{F}_1, \tag{16a}$$

$$\partial_t\overline{b}_2(\overline{y})-\nabla\cdot\left(\overline{A}_{21}(\overline{y})\nabla\overline{y}_1+\overline{A}_{22}(y)\nabla\overline{y}_2\right)=\overline{F}_2, \tag{16b}$$

with $\overline{F}_1\coloneqq F^w/\varrho_{\mathrm{l}}^{\mathrm{std}}$, $\overline{F}_2\coloneqq F^h/(C_hp_0)$ and letting $\overline{s}_{\mathrm{g}}(\overline{y})=\pi^{-1}(p_0(\overline{y}_2-\overline{y}_1))$,

$$\overline{b}_1(\overline{y})=-\Phi\overline{s}_{\mathrm{g}}(\overline{y}), \tag{17a}$$

$$\overline{b}_2(\overline{y})=\Phi a\left(\overline{s}_{\mathrm{g}}(\overline{y})\right)\overline{y}_2, \tag{17b}$$

$$\overline{A}_{11}(\overline{y})=p_0K\lambda_{\mathrm{l}}\left(1-\overline{s}_{\mathrm{g}}(\overline{y})\right), \tag{17c}$$

$$\overline{A}_{12}(\overline{y})=-\left(C_hp_0/\varrho_{\mathrm{l}}^{\mathrm{std}}\right)\Phi\left(1-\overline{s}_{\mathrm{g}}(\overline{y})\right)D_{\mathrm{l}}^h, \tag{17d}$$

$$\overline{A}_{21}(\overline{y})=\overline{y}_2p_0K\lambda_{\mathrm{l}}\left(1-\overline{s}_{\mathrm{g}}(\overline{y})\right), \tag{17e}$$

$$\overline{A}_{22}(\overline{y})=\overline{y}_2p_0K\lambda_{\mathrm{g}}\left(\overline{s}_{\mathrm{g}}(\overline{y})\right)\omega+\Phi\left(1-\overline{s}_{\mathrm{g}}(\overline{y})\right)D_{\mathrm{l}}^h, \tag{17f}$$

where $\overline{b}_i(\overline{y})$ is nondimensional and $\overline{A}_{ij}(\overline{y})$ scales as square meters per second. The matrix $\overline{A}$ yields a positive definite quadratic form (and hence ellipticity on the space differential operator) if and only if

$$4\overline{A}_{11}\overline{A}_{22}-\left(\overline{A}_{12}+\overline{A}_{21}\right)^2>0. \tag{18}$$

For applications related to hydrogen migration in underground repositories, typical values are $p_0=1$ MPa, $C_hp_0=1.5\times10^{-2}$ kg/m^3, and using the values listed in Table 1, we obtain the estimates (in square meters per second) $\overline{A}_{11}\approx5\times10^{-11}$, $\overline{A}_{12}\approx6.8\times10^{-15}$, $\overline{A}_{21}\approx5\times10^{-11}$, $\overline{A}_{22}\approx4.5\times10^{-10}$ (for $\overline{A}_{22}$, only the second term is used for the estimate, but the first term can take much larger values if the gas phase is present). Hence, condition 18 holds true. We observe that $\overline{A}_{12}\ll\overline{A}_{11}$, whence, neglecting $\overline{A}_{12}$ (and using only the second term for $\overline{A}_{22}$), we infer from Eq. 18 the condition $p_0K\lambda_{\mathrm{l}}(1)<4\Phi D_{\mathrm{l}}^h$ for ellipticity. In situations where this condition fails (e.g., because K is too large or D_{l}^h too small), a smallness condition on the dissolved hydrogen density can be invoked, with an upper bound typically depending on K and D_{l}^h. Finally, an important result under the assumption $\overline{A}_{12}\approx0$ is that the change of variables (see Smaï [33, 34])

$$\overline{y}_1=\overline{u}_1+\omega^{-1}e^{\omega\overline{u}_2},\qquad \overline{y}_2=e^{\omega\overline{u}_2}, \tag{19}$$

yields a new system in the variables $(\overline{u}_1,\overline{u}_2)$ fitting the framework of the Alt–Luckhaus theorem for the existence of weak solutions [2], namely the time-derivative term involves the gradient of a convex potential and the space-derivative terms yield a symmetric positive definite matrix.

3 Numerical method

In this section, we first present the time discretization together with the linearization procedure and then describe the dG method for space discretization. We consider the nondimensional form (Eq. 16); to alleviate the notation, bars are henceforth omitted.

3.1 Time discretization and linearization

Let $\{t^m\}_{0\le m\le M}$ be a partition of time interval $[0, T]$ such that $t^0 = 0$ and $t^M = T$, the given simulation time, and set $\tau^m = t^m - t^{m-1}$ for $m = 1, \dots, M$. Time discretization of Eq. 12 is achieved using the backward Euler method: Starting from the initial condition $y^0 := y_0$, we seek, for all $m = 1, \dots, M$, the function y^m such that, for all $i \in \{1, 2\}$,

$$\frac{1}{\tau^m}\left(b_i(y^m) - b_i(y^{m-1})\right) - \sum_{j\in\{1,2\}} \nabla\cdot\left(A_{ij}(y^m)\nabla y_j^m\right) = F_i^m,$$

where a superscript m on any problem data (e.g., on F_i) indicates evaluation at the discrete time t^m.

The linearization procedure is based on an incomplete Newton solver. It first involves a fixed-point iteration (indicated by an index l) on the coefficients in the diffusive terms, leading to

$$\frac{1}{\tau^m}\left(b_i\left(y_{l+1}^m\right) - b_i(y^{m-1})\right) - \sum_{j\in\{1,2\}} \nabla\cdot\left(A_{ij}\left(y_l^m\right)\nabla y_{j,l+1}^m\right) = F_i^m.$$

The fixed-point iteration is initialized with the values at the previous time step, i.e., we take $y_0^m := y^{m-1}$. The second ingredient in the linearization procedure is a linear approximation of the time-derivative terms,

$$\begin{aligned}
&\frac{1}{\tau^m}\left(b_i\left(y_{l+1}^m\right) - b_i(y^{m-1})\right)\\
&\quad= \frac{1}{\tau^m}\left(b_i\left(y_{l+1}^m\right) - b_i\left(y_l^m\right)\right)\\
&\qquad+\frac{1}{\tau^m}\left(b_i\left(y_l^m\right) - b_i(y^{m-1})\right)\\
&\quad\approx \partial_1 b_i\left(y_l^m\right)\frac{y_{1,l+1}^m - y_{1,l}^m}{\tau^m} + \partial_2 b_i\left(y_l^m\right)\frac{y_{2,l+1}^m - y_{2,l}^m}{\tau^m}\\
&\qquad+\frac{b_i\left(y_l^m\right) - b_i(y^{m-1})}{\tau^m}.
\end{aligned}$$

As a result, for all $m = 1, \dots, M$ (time loop) and for all $l \ge 0$ (fixed-point loop), we seek y_{l+1}^m such that, for all $i \in \{1, 2\}$,

$$\begin{aligned}
&-\sum_{j\in\{1,2\}} \nabla\cdot\left(A_{ij}\left(y_l^m\right)\nabla y_{j,l+1}^m\right) + \sum_{j\in\{1,2\}} \partial_j b_i\left(y_l^m\right)\frac{y_{j,l+1}^m - y_{j,l}^m}{\tau^m}\\
&\quad= F_i^m - \frac{b_i(y_l^m) - b_i(y^{m-1})}{\tau^m}.
\end{aligned}$$

Solving for y_{l+1}^m amounts to solving the linear system of PDEs,

$$\begin{aligned}
&-\nabla\cdot\left(A_{11}\left(y_l^m\right)\nabla y_{1,l+1}^m + A_{12}\left(y_l^m\right)\nabla y_{2,l+1}^m\right)\\
&\qquad+\frac{1}{\tau^m}\left(\partial_1 b_1\left(y_l^m\right) y_{1,l+1}^m + \partial_2 b_1\left(y_l^m\right) y_{2,l+1}^m\right) = G_{1,l}^m,
\end{aligned} \tag{20a}$$

$$\begin{aligned}
&-\nabla\cdot\left(A_{21}\left(y_l^m\right)\nabla y_{1,l+1}^m + A_{22}\left(y_l^m\right)\nabla y_{2,l+1}^m\right)\\
&\qquad+\frac{1}{\tau^m}\left(\partial_1 b_2\left(y_l^m\right) y_{1,l+1}^m + \partial_2 b_2\left(y_l^m\right) y_{2,l+1}^m\right) = G_{2,l}^m,
\end{aligned} \tag{20b}$$

with the right-hand sides, for all $i \in \{1, 2\}$,

$$\begin{aligned}
G_{i,l}^m = F_i^m &+ \frac{1}{\tau^m} b_i(y^{m-1})\\
&+\frac{1}{\tau^m}\left(\partial_1 b_i\left(y_l^m\right) y_{1,l}^m + \partial_2 b_i\left(y_l^m\right) y_{2,l}^m - b_i\left(y_l^m\right)\right),
\end{aligned} \tag{21}$$

together with the boundary conditions

$$y_{l+1}^m = y_{\mathrm{D}}^m \qquad \text{on } \partial\Omega_{\mathrm{D}}, \tag{22a}$$

$$\mathbf{n}\cdot\boldsymbol{\sigma}_i(y_{l+1}^m) = \sigma_i^m,\ i \in \{1, 2\},\ \text{on } \partial\Omega_{\mathrm{N}}. \tag{22b}$$

3.2 Space discretization: dG method

Let $\{\mathcal{T}_\delta\}_{\delta>0}$ be a family of shape-regular meshes of the domain Ω (possibly containing hanging nodes), where δ denotes the maximum element diameter in $\mathcal{T}_\delta$. We say that the set F is a mesh interface (resp., boundary face) if F has nonzero $(d-1)$-dimensional measure and if there exist distinct $T^-, T^+ \in \mathcal{T}_\delta$ such that $F = \partial T^- \cap \partial T^+$ (resp., if there exists $T \in \mathcal{T}_\delta$ such that $F = \partial T \cap \partial\Omega$). Interfaces are collected in the set $\mathcal{F}_\delta^{\mathrm{i}}$, boundary faces in the set $\mathcal{F}_\delta^{\mathrm{b}}$, and we let $\mathcal{F}_\delta := \mathcal{F}_\delta^{\mathrm{b}} \cup \mathcal{F}_\delta^{\mathrm{i}}$. For all $F \in \mathcal{F}_\delta$, δ_F denotes its diameter. We suppose that the

meshes $\mathcal{T}_\delta$ are fitted to the partition $\partial\Omega = \partial\Omega_D \cup \partial\Omega_N$; accordingly, the set of boundary faces $\mathcal{F}_\delta^b$ is partitioned as $\mathcal{F}_\delta^b = \mathcal{F}_\delta^D \cup \mathcal{F}_\delta^N$ with obvious notation.

For a scalar- or vector-valued function v that is possibly two-valued at an interface $F = \partial T^- \cap \partial T^+ \in \mathcal{F}_\delta^i$, we define its jump and average at F as

$$[\![v]\!] = v^- - v^+, \quad \{v\} = \tfrac{1}{2}(v^- + v^+), \quad v^\pm = v|_{T^\pm}$$

and extend these definitions to boundary faces $F = \partial T \cap \partial\Omega \in \mathcal{F}_\delta^b$ by setting $[\![v]\!] = \{v\} = v|_T$. For all $F = \partial T^- \cap \partial T^+ \in \mathcal{F}_\delta^i$, we define $\mathbf{n}_F$ as the unit normal vector to F pointing from T^- toward T^+, whereas for $F \in \mathcal{F}_\delta^b$ we set $\mathbf{n}_F = \mathbf{n}$. The sign arbitrariness in the definition of $\mathbf{n}_F$ and of the jump across F, for all $F \in \mathcal{F}_\delta^i$, is irrelevant in what follows.

Let $k \geq 1$ be an integer. The dG method is based on the discrete space

$$V_\delta^k := \left\{ v_\delta \in L^2(\Omega);\ \forall T \in \mathcal{T}_\delta,\ v_\delta|_T \in \mathbb{P}_k(T) \right\}, \tag{23}$$

where $\mathbb{P}_k(T)$ denotes the vector space spanned by polynomials of total degree $\leq k$ on T. Let $y_\delta \in [V_\delta^k]^2$ and let $i, j \in \{1, 2\}$. The interior penalty dG bilinear form discretizing the differential operator $-\nabla \cdot (A_{ij}(y_\delta)\nabla\cdot)$ can be written, for all $u_\delta, v_\delta \in V_\delta^k$, as

$$\begin{aligned} a_\delta^{ij}(y_\delta; u_\delta, v_\delta) = & \sum_{T\in\mathcal{T}_\delta} \int_T A_{ij}(y_\delta)\nabla u_\delta \cdot \nabla v_\delta \\ & - \sum_{F\in\mathcal{F}_\delta^i\cup\mathcal{F}_\delta^D} \int_F \mathbf{n}_F\cdot\{A_{ij}(y_\delta)\nabla u_\delta\}[\![v_\delta]\!] \\ & -\theta^{ij} \sum_{F\in\mathcal{F}_\delta^i\cup\mathcal{F}_\delta^D} \int_F \mathbf{n}_F\cdot\{A_{ij}(y_\delta)\nabla v_\delta\}[\![u_\delta]\!] \\ & + \sum_{F\in\mathcal{F}_\delta^i\cup\mathcal{F}_\delta^D} \eta_F^{ij}\frac{\sigma k^2}{\delta_F}\int_F [\![u_\delta]\!][\![v_\delta]\!], \end{aligned}$$

where $\theta^{ij} = 0$ for $i \neq j$ and $\theta^{ii} = 1$ for $i \in \{1, 2\}$ (so that the diagonal blocks of the linear system matrix remain symmetric), while $\eta^{ij} = 0$ for $i \neq j$ and $\eta_F^{ii} = \|A_{ii}\|_{L^\infty(\Omega)}$ for $i \in \{1, 2\}$ (in the present context, the variations of A_{ii} in Ω are sufficiently mild to use a global scaling for the penalty parameter). Moreover, the user-dependent parameter σ is typically set to 10.

We consider the following dG method: Given $y_\delta^{m-1} \in [V_\delta^k]^2$ from the previous time step (or the L^2-projection of the initial condition), the fixed-point loop is initialized as $y_{\delta,0}^m = y_\delta^{m-1}$, and, for all $l \geq 0$, we seek $y_{\delta,l+1}^m \in [V_\delta^k]^2$ such that, for all $v_\delta, w_\delta \in V_\delta^k$,

$$\begin{aligned} & a_\delta^{11}\left(y_{\delta,l}^m; y_{1,\delta,l+1}^m, v_\delta\right) + a_\delta^{12}\left(y_{\delta,l}^m; y_{2,\delta,l+1}^m, v_\delta\right) \\ & \quad + \frac{1}{\tau^m}\int_\Omega \Big(\partial_1 b_1\left(y_{\delta,l}^m\right) y_{1,\delta,l+1}^m + \partial_2 b_1\left(y_{\delta,l}^m\right) y_{2,\delta,l+1}^m\Big) v_\delta \\ & \quad = \int_\Omega G_{1,l}^m v_\delta - \sum_{F\in\mathcal{F}_\delta^N}\int_F \sigma_1^m v_\delta \\ & \qquad + \sum_{F\in\mathcal{F}_\delta^D}\int_F \Big(\phi_F^{11}\left(y_{\delta,l}^m; v_\delta\right) y_{1,D}^m + \phi_F^{12}\left(y_{\delta,l}^m; v_\delta\right) y_{2,D}^m\Big), \end{aligned} \tag{24}$$

$$\begin{aligned} & a_\delta^{21}\left(y_{\delta,l}^m; y_{1,\delta,l+1}^m, w_\delta\right) + a_\delta^{22}\left(y_{\delta,l}^m; y_{2,\delta,l+1}^m, w_\delta\right) \\ & \quad + \frac{1}{\tau^m}\int_\Omega \Big(\partial_1 b_2\left(y_{\delta,l}^m\right) y_{1,\delta,l+1}^m + \partial_2 b_2\left(y_{\delta,l}^m\right) y_{2,\delta,l+1}^m\Big) w_\delta \\ & \quad = \int_\Omega G_{2,l}^m w_\delta - \sum_{F\in\mathcal{F}_\delta^N}\int_F \sigma_2^m w_\delta \\ & \qquad + \sum_{F\in\mathcal{F}_\delta^D}\int_F \Big(\phi_F^{21}\left(y_{\delta,l}^m; w_\delta\right) y_{1,D}^m + \phi_F^{22}\left(y_{\delta,l}^m; w_\delta\right) y_{2,D}^m\Big), \end{aligned} \tag{25}$$

with $\phi_F^{ij}(y_\delta; v_\delta) = -\theta^{ij}\mathbf{n}_F\cdot A_{ij}(y_\delta)\nabla v_\delta + \eta_F^{ij}\frac{\sigma k^2}{\delta_F} v_\delta$, for all $i, j \in \{1, 2\}$. Integrating by parts elementwise the volume term in the bilinear forms a_δ^{ij}, it is seen that the above formulation weakly enforces the PDEs (Eq. 11) in each mesh element, the boundary conditions (Eq. 22) on all boundary faces, and, on all mesh interfaces $F \in \mathcal{F}_\delta^i$, the transmission conditions

$$[\![y_i]\!] = 0, \qquad \mathbf{n}_F \cdot [\![\boldsymbol{\sigma}_i(y)]\!] = 0, \qquad \forall i \in \{1, 2\}, \tag{26}$$

consistently with the properties satisfied by the exact solution.

Remark 1 For heterogeneous media consisting of different rocks with contrasting properties, weighted averages can be considered in the formulation of the dG method, as in [11, 17] for linear advection–diffusion equations. Furthermore, we observe that Eq. 26 implies that the dissolved hydrogen density ϱ_l^h is continuous at any interface. Owing to Henry's law, the gas pressure (if this phase exists on both sides of the interface) is also continuous; hence, since the liquid pressure is continuous (also by Eq. 26), the capillary pressure is also continuous at the interface. However, the gas saturation is in general discontinuous at the interface; this fact is illustrated in the test case of Section 4.3. Instead,

for two-component porous media flows without interphase mass exchange where one of the saturations is used as one of the main unknowns, the penalty strategy in the dG method must be revised to enforce weakly a nonlinear jump condition on the saturation, cf. [16].

4 Numerical results

In this section, we evaluate numerically the dG method derived in Section 3 on three one-dimensional test cases, dedicated respectively to gas-phase (dis)appearance, ill-prepared initial conditions, and heterogeneous problems with different rock types. The first two test cases have been proposed within the GNR MoMaS in connection with the Couplex-Gas benchmark proposed by the French National Radioactive Waste Management Agency; reference solutions can be found in [19]. The third test case has been investigated in [9].

We use the van Genuchten model for capillary pressure and the van Genuchten–Mualem model for relative permeability, i.e.,

$$\pi(s_{\mathrm{g}}) = P_{\mathrm{r}}\left(s_{\mathrm{le}}(s_{\mathrm{g}})^{-1/m} - 1\right)^{1/n}, \tag{27a}$$

$$\lambda_l(s_{\mathrm{g}}) = \frac{1}{\mu_{\mathrm{l}}} s_{\mathrm{le}}(s_{\mathrm{g}})^{1/2}\left(1 - \left(1 - s_{\mathrm{le}}(s_{\mathrm{g}})^{1/m}\right)^m\right)^2, \tag{27b}$$

$$\lambda_g(s_{\mathrm{g}}) = \frac{1}{\mu_{\mathrm{g}}} s_{\mathrm{ge}}(s_{\mathrm{g}})^{1/2}\left(1 - s_{\mathrm{le}}(s)^{1/m}\right)^{2m}, \tag{27c}$$

where $m = 1 - \frac{1}{n}$, μ_{l} and μ_{g} are viscosities, while

$$s_{\mathrm{ge}}(s_{\mathrm{g}}) = \frac{s_{\mathrm{g}} - s_{\mathrm{gr}}}{1 - s_{\mathrm{lr}} - s_{\mathrm{gr}}}, \qquad s_{\mathrm{le}}(s_{\mathrm{g}}) = 1 - s_{\mathrm{ge}}(s_{\mathrm{g}}), \tag{28}$$

are the relative gas and liquid saturations and s_{gr}, s_{lr} are the residual saturations in the gas and liquid phases, respectively. Values for the above physical parameters are specified below for each test case. In all cases, the convergence criterion in the incomplete Newton method uses a tolerance of 10^{-8} in the $L^2(\Omega)$-norm, and in the present one-dimensional setting, a direct solver is used for the linear systems.

4.1 Gas-phase (dis)appearance

In this test case, hydrogen is injected into the porous medium $\Omega = (0, 200)$ m initially saturated by water. Injection is performed through the left boundary $x = 0$ during the injection time $T_{\mathrm{inj}} = 10^5$ year, while the simulation time is $T = 10^6$ years. There are no external sources, i.e., $F^w = F^h = 0$. This example illustrates the potential of the method to simulate gas-phase appearance and disappearance related to hydrogen injection.

The porous medium and fluid characteristics are presented in Table 1. Initial and boundary conditions are given by

$$-\mathbf{n}\cdot\boldsymbol{\sigma}_1|_{x=0} = 0, \qquad -\mathbf{n}\cdot\boldsymbol{\sigma}_2|_{x=0} = q_{\mathrm{inj}}; \tag{29}$$

$$p_{\mathrm{l}}|_{x=200} = 10^6\ \mathrm{Pa}, \qquad \varrho_{\mathrm{l}}^h|_{x=200} = 0; \tag{30}$$

$$p_{\mathrm{l}}|_{t=0} = 10^6\ \mathrm{Pa}, \qquad \varrho_{\mathrm{l}}^h|_{t=0} = 0; \tag{31}$$

where $q_{\mathrm{inj}} = 5.57\times10^{-6}\chi_{[0,T_{\mathrm{inj}}]}(t)$ kg/m^2/year and χ_A denotes the characteristic function of the set A. The ellipticity criterion (Eq. 18) can be verified at each point in space and in time; the left-hand side of Eq. 18 takes values in the range $[1, 8]\times10^{-4}$ (m^2/year)^2.

We consider the first-order dG space V_δ^1 ($k = 1$) and use a uniform mesh of 200 elements in Ω. In time, we consider the partition $[0, 1, 2, 3, 5, 7, 10]\times10^5$ years of the time interval $[0, T]$ and use the time steps $\tau = [125, 500, 1{,}000, 5{,}000, 1{,}000, 5{,}000]$ years within each time slab.

Figures 2 and 3 present the selected results of our simulations at various times. During an initial transient up to $\approx 2\times10^3$ years, the dissolved hydrogen molar density increases owing to gas injection, while the liquid

Table 1 Parameter values for the porous medium and fluid characteristics used in test case 1

Porous medium			Fluid characteristics		
Parameter	Value		Parameter	Value	
Φ	0.15	(–)	D_{l}^h	3×10^{-9}	m^2/s
K	5×10^{-20}	m^2	μ_{l}	1×10^{-3}	Pa s
P_{r}	2×10^6	Pa	μ_{g}	9×10^{-6}	Pa s
n	1.49	(–)	$H(303K)$	7.65×10^{-6}	mol/Pa/m^3
s_{lr}	0.4	(–)	M^h	2×10^{-3}	kg/mol
s_{gr}	0	(–)	$\varrho_{\mathrm{l}}^{\mathrm{std}}$	10^3	kg/m^3

pressure remains roughly constant, and there is no gas phase. The gas phase appears at the time $\approx 1.3\times 10^4$ years, and the liquid pressure begins to increase until it reaches its maximum at the time $\approx 10^5$ years. The gas saturation continues to increase up to the time $\approx 5\times 10^5$ years, while the gas pressure reaches its maximum at $x = 0$ at the time $\approx 10^5$ years and decreases afterward. When the gas injection is eventually

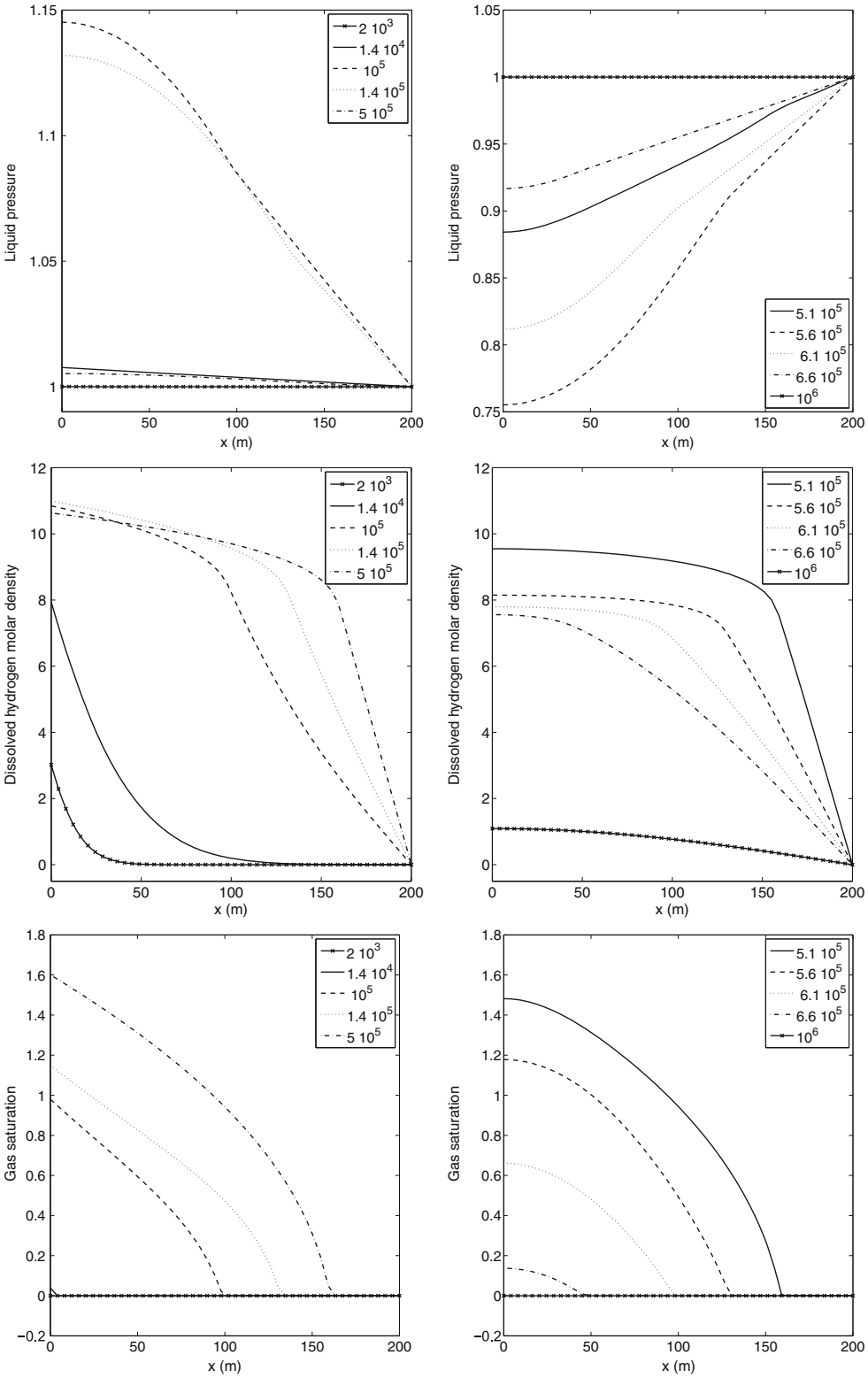

Fig. 2 Liquid pressure p_l (*top line*, megapascal), dissolved hydrogen molar density ϱ_l^h / M^h (*second line*, moles per cubic meter), and gas saturation s_g (*bottom line*, percent) at times $\{2\times 10^3, 1.4\times 10^4, 10^5, 1.4\times 10^5, 5\times 10^5\}$ (*left column*, years) and $\{5.1\times 10^5, 5.6\times 10^5, 6.1\times 10^5, 6.6\times 10^5, 10^6\}$ (*right column*, years)

stopped, the liquid pressure starts to decrease (owing to the absence of entering water flux at $x = 0$) and reaches its minimum at the time $\approx 5.6 \times 10^5$ years. Afterward, the water pressure increases again, the dissolved hydrogen molar density and the gas saturation decrease, while the system has almost reached equilibrium at the final simulation time. All these results agree well with those presented in [19, 32].

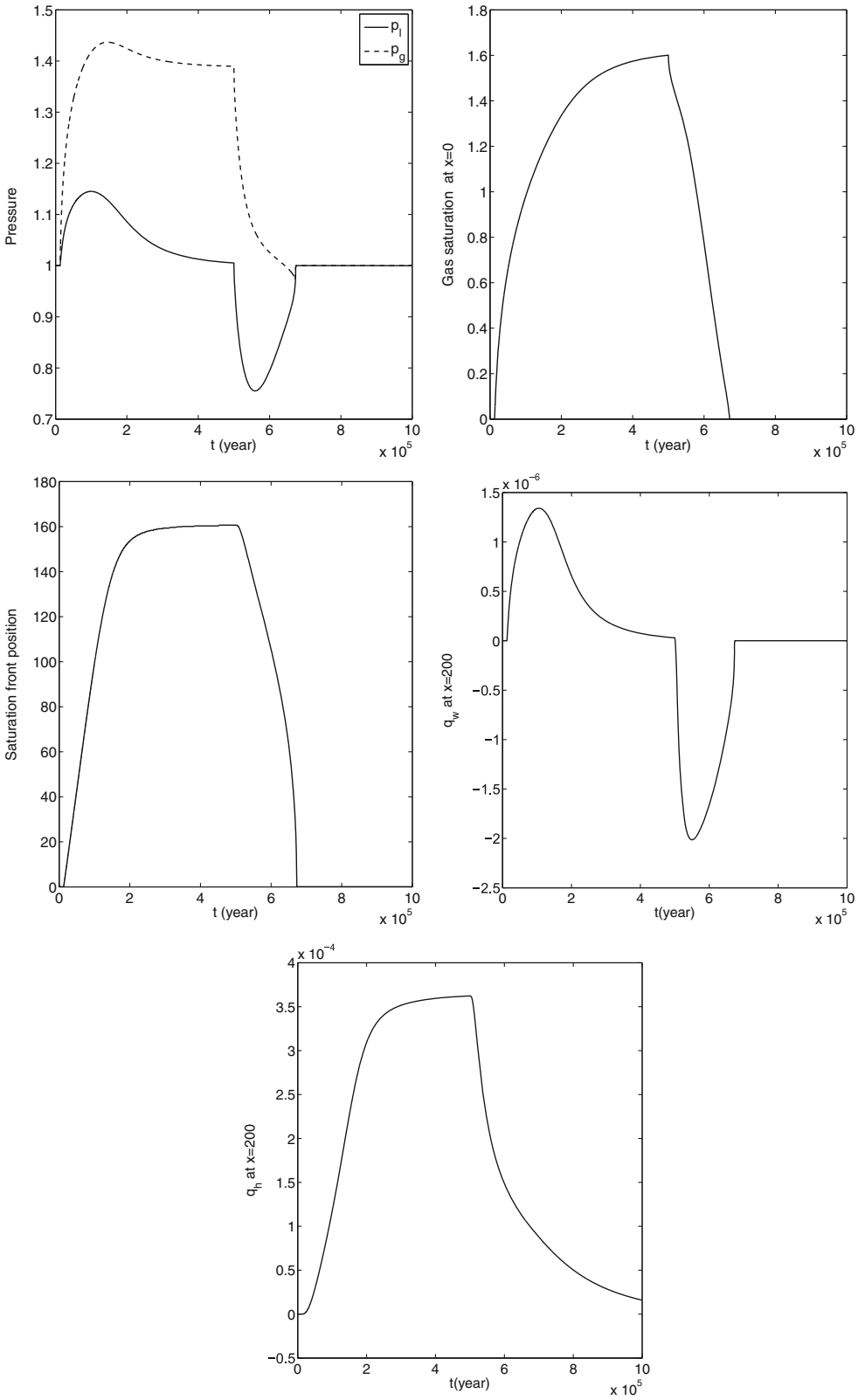

Fig. 3 From *top* to *bottom* and from *left* to *right*, as a function of time: liquid and gas pressures p_l and p_g at $x = 0$ (megapascal), gas saturation s_g at $x = 0$ (percent), front position of the gas phase (meters), total water flux at $x = 200$ (kilogram per square meter per year), and total hydrogen flux at $x = 200$ (kilogram per square meter per year)

4.2 Ill-prepared initial condition

In this test case, we consider the domain $\Omega = (0, 1)$ m with zero flux boundary conditions and no external sources, while uniform liquid pressure and discontinuous gas pressure are considered as initial conditions. Owing to the discontinuity of the gas pressure, the system is initially out of the mechanical equilibrium. This example illustrates the potential of the method to simulate the evolution of the system back to equilibrium starting from an ill-prepared initial condition.

The porous medium and fluid characteristics are presented in Table 2. The main difference with Table 1 is the higher value for K. Initial and boundary conditions are given by

$$-\mathbf{n}\cdot\boldsymbol{\sigma}_1|_{x=0} = 0, \quad -\mathbf{n}\cdot\boldsymbol{\sigma}_2|_{x=0} = 0;$$
$$-\mathbf{n}\cdot\boldsymbol{\sigma}_1|_{x=1} = 0, \quad -\mathbf{n}\cdot\boldsymbol{\sigma}_2|_{x=1} = 0;$$
$$p_l(x, 0) = 10^6 \text{ Pa}, \quad x \in (0, 1)$$
$$p_g(x, 0) = \begin{cases} 1.5\times10^6 \text{ Pa} & \text{if } x \in (0, 0.5), \\ 2.5\times10^6 \text{ Pa} & \text{if } x \in (0.5, 1). \end{cases}$$

The left-hand side of Eq. 18 takes values in the range $[6, 9] \times 10^3$ $(\text{m}^2/\text{year})^2$.

We consider the first-order dG space V_δ^1 $(k = 1)$ and use a uniform mesh of 512 elements in Ω. The simulation time is $T = 10^6$ s. We consider the partition $T = [0, 10, 10^2, 5\times10^2, 10^3, 5\times10^3, 10^4, 2\times10^5, 5\times10^5, 10^6]$ s of the time interval $[0, T]$ and use 32 uniform time steps within each time slab.

Figures 4 and 5 present selected results of our simulations at various times. The gas phase is initially present in the whole domain. Owing to the initial discontinuity in the gas pressure, the gas saturation and the dissolved hydrogen density are also discontinuous initially. After a short time (10 s), the liquid pressure exhibits a jump of the order of 0.8 MPa. Then, a liquid pressure front propagates and reaches the boundaries at $\approx10^2$ s. Afterward, up to the time $\approx10^4$ s, the liquid pressure increases at the left boundary and decreases at the right boundary. At the time $\approx10^4$ s, the difference of left and right boundary values is of the order of 1 MPa, and the liquid pressure still exhibits a sharp gradient at $x = 0.5$. Next, the difference between boundary values begins to decrease, and the liquid pressure smoothly converges to its equilibrium position, which it has almost reached at time 10^6 s. Furthermore, the initially discontinuous profile of dissolved hydrogen density is smoothed owing to fast hydrogen diffusion in water. Thus, this profile reaches equilibrium much earlier than the liquid pressure, at time $\approx10^4$ s. Finally, the gas saturation profile exhibits a very steep front up to the time $\approx10^3$ s; then, the shock slowly dissipates, but the profile still exhibits a sizable gradient at time $\approx10^5$ s. The gas saturation profile has almost relaxed back to equilibrium at the final simulation time. All these results agree well with those reported in [19].

4.3 Hydrogen injection in heterogeneous medium

In this test case, we consider the heterogeneous porous medium $\Omega = (0, 200)$ m composed of two rocks occupying, respectively, the subdomains $\Omega_1 = (0, 20)$ and $\Omega_2 = (20, 200)$. The porous medium and fluid characteristics are presented in Table 3. The column for the porous medium contains two values, one for each rock type. We observe that the rock occupying the subdomain Ω_2 has a finer texture.

As in test case 1, the initial and boundary conditions are given by Eq. 31, except that the gas injection is not stopped at time T_{inj}. This example illustrates the potential of the method to handle heterogeneous porous media. The left-hand side of Eq. 18 takes values in the range $[10^{-4}, 1]$ $(\text{m}^2/\text{year})^2$.

We consider the first-order dG space V_δ^1 $(k = 1)$ and use a uniform mesh of 16 elements in Ω_1 and 144 elements in Ω_2 so that the mesh is fitted to the interface separating Ω_1 and Ω_2. The simulation time is $T = 10^6$ years. We consider the partition $[0, 6\times10^4, 2\times10^5,$

Table 2 Parameter values for the porous medium and fluid characteristics used in test case 2

Porous medium			Fluid characteristics		
Parameter	Value		Parameter	Value	
Φ	0.3	(–)	D_l^h	3×10^{-9}	m^2/s
K	10^{-16}	m^2	μ_l	1×10^{-3}	Pa s
P_r	2×10^6	Pa	μ_g	9×10^{-6}	Pa s
n	1.54	(–)	$H(303K)$	7.65×10^{-6}	mol/Pa/m^3
s_{lr}	0.01	(–)	M^h	2×10^{-3}	kg/mol
s_{gr}	0	(–)	ϱ_l^{std}	10^3	kg/m^3

6×10^5, 10^6] years of the time interval $[0, T]$ and use the time steps $\tau = [200, 1{,}000, 2{,}000, 20{,}000]$ years within each time slab. We recall that the dG method weakly enforces the continuity of the normal component of the total fluxes and that of the liquid pressure and of the dissolved hydrogen density, cf. Eq. 26.

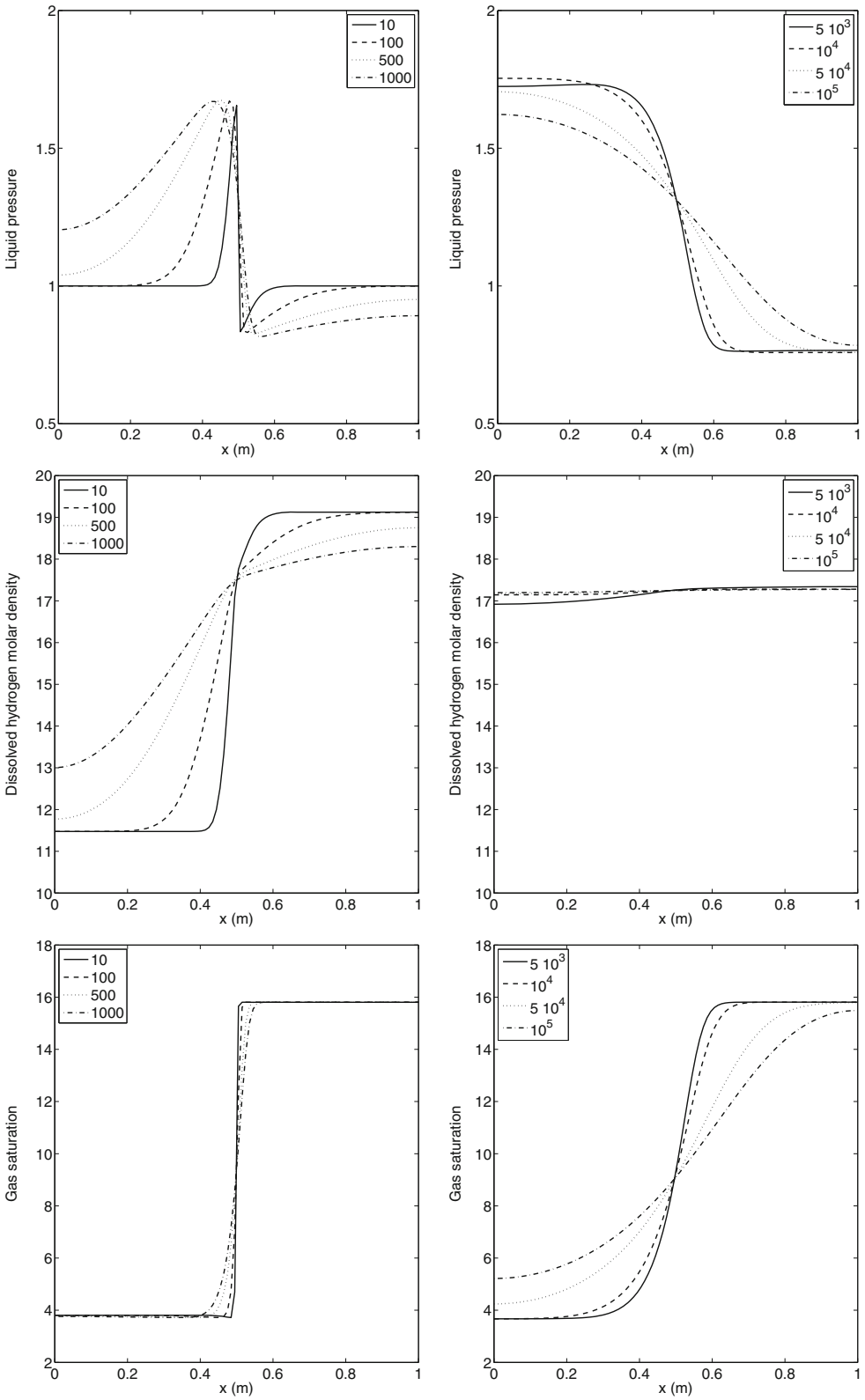

Fig. 4 Liquid pressure p_l (*top line*, megapascal), dissolved hydrogen molar density ϱ_l^h / M^h (*second line*, moles per cubic meter), and gas saturation s_g (*bottom line*, percent) at times $\{10, 10^2, 5\times10^2, 10^3\}$ (*left column*, second) and $\{5\times10^3, 10^4, 5\times10^4, 10^5\}$ (*right column*, second)

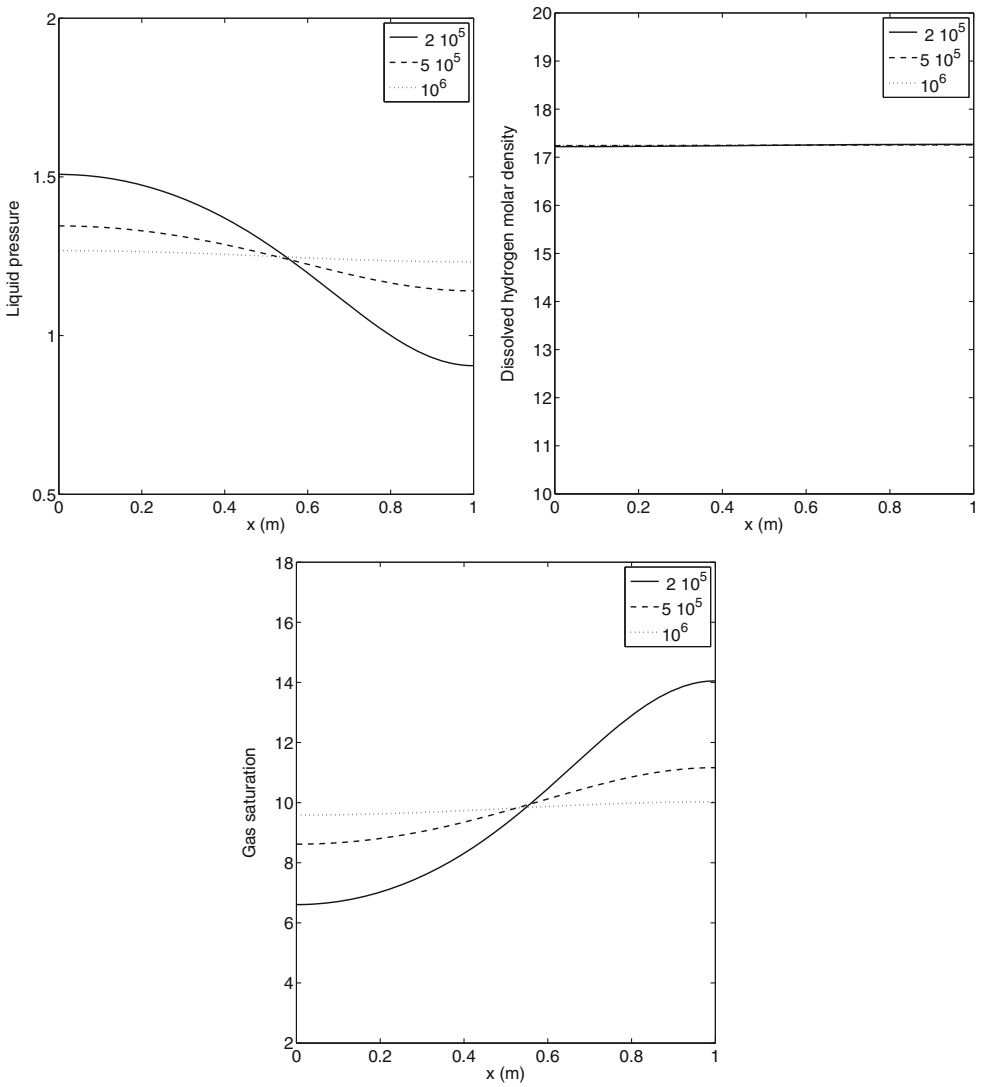

Fig. 5 Liquid pressure p_l (megapascal), dissolved hydrogen molar density ϱ_h^l / M^h (moles per cubic meter), and gas saturation s_g (percent) at times $\{2\times10^5, 5\times10^5, 10^6\}$ s

Figure 6 presents selected results of our simulations at various times. Owing to gas injection, the gas phase appears in the first subdomain at the time $\approx 3\times10^4$ years and reaches the interface separating the two rock types at the time $\approx 4.2\times10^4$ years. The saturation at the left of the interface (in the coarser rock) starts to increase while maintaining the jump in the saturation such that capillary pressure continuity is preserved, and the gas phase penetrates into the second (finer) rock. Next, at the time $\approx 1.3\times10^5$ years, the liquid pressure starts to decrease, and the system relaxes back to equilibrium, as reflected by the fact that the net difference of total hydrogen flow at inflow and outflow boundaries tends to zero. We stress that the capillary

Table 3 Parameter values for the porous medium and fluid characteristics used in test case 3

Porous medium			Fluid characteristics		
Parameter	Value		Parameter	Value	
Φ	(0.3, 0.15)	(-)	D_l^h	3×10^{-9}	m^2/s
K	$(10^{-18}, 5 \times 10^{-20})$	m^2	μ_l	1×10^{-3}	Pa s
P_r	$(2 \times 10^6, 15 \times 10^6)$	Pa	μ_g	9×10^{-6}	Pa s
n	(1.54, 1.49)	(-)	$H(303K)$	7.65×10^{-6}	mol/Pa/m^3
s_{lr}	(0.01, 0.4)	(-)	M^h	2×10^{-3}	kg/mol
s_{gr}	(0, 0)	(-)	ϱ_l^{std}	10^3	kg/m^3

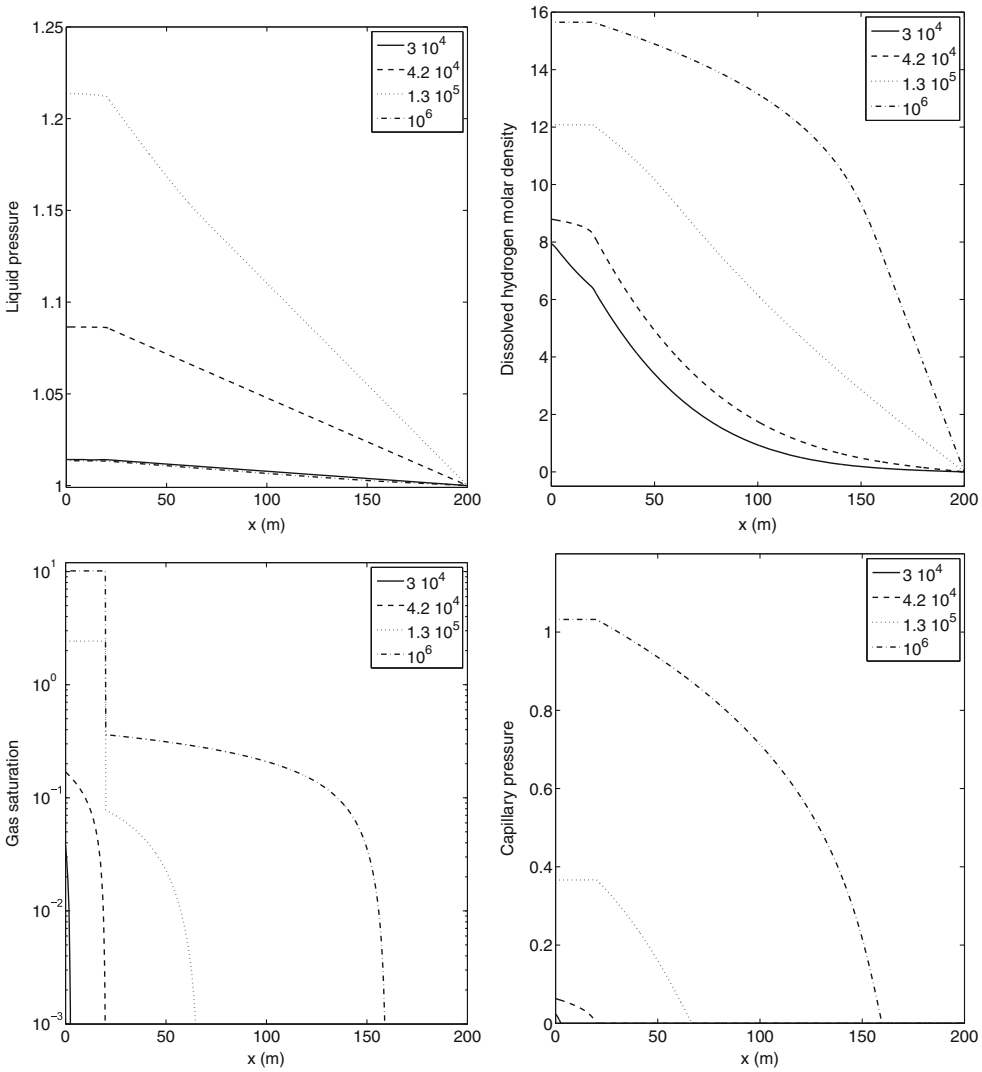

Fig. 6 Liquid pressure p_l (megapascal), dissolved hydrogen molar density ϱ_l^h / M^h (moles per cubic meter), gas saturation s_g (percent), and capillary pressure π (megapascal) at times $\{3\times10^4, 4.2\times10^4, 1.3\times10^5, 10^6\}$ (years)

pressure is continuous at the interface at all times. The results are in good agreement with those reported in [9].

5 Conclusions

The above numerical results show that the proposed methodology is capable of delivering accurate discrete solutions capturing the correct physical behavior in various complex situations. Future work can aim at assessing the proposed methodology on higher-dimensional test cases and at analyzing the discrete scheme to derive stability and error estimates.

Acknowledgments The authors are grateful to Farid Smaï (IRSN) for fruitful discussions. This study was partially supported by the Groupement MoMaS (PACEN/CNRS, ANDRA, BRGM, CEA, EdF, IRSN), France and by CNPq, Brazil.

References

1. Abadpour, A., Panfilov, M.: Method of negative saturations for multiple compositional flow with oversaturated zones. Transp. Porous Media **79**, 197–214 (2010)
2. Alt, H.W., Luckhaus, S.: Quasilinear elliptic–parabolic differential equations. Math. Z. **183**(3), 311–341 (1983)
3. Amaziane, B., Jurak, M., Žgaljić Keko, A.: An existence result for a coupled system modeling a fully equivalent global pressure formulation for immiscible compressible two-phase flow in porous media. J. Differ. Equ. **250**(3), 1685–1718 (2011)
4. Arnold, D.N., Brezzi, F., Cockburn, B., Marini, L.D.: Unified analysis of discontinuous Galerkin methods for elliptic problems. SIAM J. Numer. Anal. **39**(5), 1749–1779 (2002)
5. Bastian, P., Rivière, B.: Discontinuous Galerkin methods for two-phase flow in porous media. Technical Report 2004-28 (2004)
6. Bear, J.: Dynamic of Fluids in Porous Media. Dover, New York (1978)
7. Benilan, P., Wittbold, P.: On mild and weak solutions of elliptic–parabolic problems. Adv. Differ. Equ. **1**(6), 1053–1073 (1996)

8. Bourgeat, A., Jurak, M., Smaï, F.: Two phase, partially miscible flow and transport modeling in porous media; application to gas migration in a nuclear waste repository. Comput. Geosci. **13**, 29–42 (2009)
9. Bourgeat, A., Jurak, M., Smaï, F.: Modelling and numerical simulation of gas migration in nuclear waste repository. arXiv:1006.2914 (2010)
10. Chavent, G., Jaffré, J.: Mathematical Models and Finite Elements for Reservoir Simulation. Elsevier, Amsterdam (1978)
11. Di Pietro, D.A., Ern, A., Guermond, J.L.: Discontinuous Galerkin methods for anisotropic semi-definite diffusion with advection. SIAM J. Numer. Anal. **46**(2), 805–831 (2008)
12. Di Pietro, D.A., Ern, A.: Mathematical Aspects of Discontinuous Galerkin Methods, Mathématiques & Applications, vol. 69. Springer, New York (2012)
13. Epshteyn, Y., Rivière, B.: Fully implicit discontinuous finite element methods for two-phase flow. Appl. Numer. Math. **57**, 383–401 (2007)
14. Ern, A., Guermond, J.L.: Discontinuous Galerkin methods for Friedrichs´ systems. I. General theory. SIAM J. Numer. Anal. **44**(2), 753–778 (2006)
15. Ern, A., Mozolevski, I., Schuh, L.: Accurate velocity reconstruction for discontinuous Galerkin approximations of two-phase porous media flows. C. R. Math. Acad. Sci. Paris **347**(9–10), 551–554 (2009)
16. Ern, A., Mozolevski, I., Schuh, L.: Discontinuous Galerkin approximation of two-phase flows in heterogeneous porous media with discontinuous capillary pressures. Comput. Methods Appl. Mech. Eng. **199**, 1491–1501 (2010)
17. Ern, A., Stephansen, A.F., Zunino, P.: A discontinuous Galerkin method with weighted averages for advection–diffusion equations with locally small and anisotropic diffusivity. IMA J. Numer. Anal. **29**(2), 235–256 (2009)
18. Eslinger, O.J.: Discontinuous Galerkin finite element methods applied to two-phase, air–water flow problems. Ph.D. thesis, University of Texas at Austin (2005)
19. GNR MoMaS: http://www.gdrmomas.org/ex_qualifications.html (2011)
20. Helmig, R.: Multiphase Flow and Transport Processes in the Subsurface. Springer, New York (1997)
21. Hesthaven, J.S., Warburton, T.: Nodal Discontinuous Galerkin Methods. Algorithms, Analysis, and Applications, Texts in Applied Mathematics, vol. 54. Springer, New York (2008)
22. Jaffré, J., Sboui, A.: Henry's law and gas phase disappearance. Transp. Porous Media **82**, 521–526 (2010)
23. Kačur, J.: On a solution of degenerate elliptic–parabolic systems in Orlicz–Sobolev spaces. I. Math. Z. **203**(1), 153–171 (1990)
24. Kačur, J.: On a solution of degenerate elliptic–parabolic systems in Orlicz–Sobolev spaces. II. Math. Z. **203**(4), 569–579 (1990)
25. Khalil, Z., Saad, M.: On a fully nonlinear degenerate parabolic system modeling immiscible gas–water displacement in porous media. Nonlinear Anal. Real World Appl. **12**(3), 1591–1615 (2011)
26. Marle, C.M.: Multiphase flow in porous media. Edition Technip, Houston (1981)
27. Mikelić, A.: An existence result for the equations describing a gas–liquid two-phase flow. C. R., Mec. **337**(4), 226–232 (2009)
28. Otto, F.: L^1-contraction and uniqueness for quasilinear elliptic–parabolic equations. J. Differ. Equ. **131**(1), 20–38 (1996)
29. Panfilov, M., Rasoulzadeh, M.: Interfaces of phase transition and disappearance and method of negative saturation for compositional flow with diffusion and capillarity in porous media. Transp. Porous Media **83**(1), 73–98 (2010)
30. Peaceman, D.W.: Fundamentals of Numerical Reservoir Simulation. Elsevier, Amsterdam (1977)
31. Rivière, B.: Discontinuous Galerkin Methods for Solving Elliptic and Parabolic Equations: Theory and Implementation. Frontiers in Mathematics. SIAM, Philadelphia (2008)
32. Smaï, F.: Développement d'outils mathématiques et numériques pour l'évaluation du concept de stockage géologique. Ph.D. thesis, Université Claude Bernard Lyon I (2009)
33. Smaï, F.: Existence of solutions for a model of multiphase flow in porous media applied to gas migration in underground nuclear waste repository. Appl. Anal. **88**(10–11), 1609–1616 (2009)
34. Smaï, F.: A model of multiphase flow and transport in porous media applied to gas migration in underground nuclear waste repository. C. R. Math. Acad. Sci. Paris **347**(9–10), 527–532 (2009)